On wind turbine power fluctuations induced by large-scale motions

Mohammad H.B. Ahmadi[a,*], Zhiyin Yang[a]

[a]*School of Computing and Engineering, University of Derby, Derby DE22 3AW, UK*

ARTICLE INFO

ABSTRACT

Our current understanding on the dynamic interaction between large-scale motions in the approaching turbulent flow and wind turbine power is very limited. To address this, numerical studies of a small-scale three-bladed horizontal axis wind turbine with cylinders placed in front of it to produce energetic coherent structures of varying scale relative to the turbine size have been carried out to examine the temporary variations of the turbine power. The predicted spectra reveal a strong interaction between large-scale turbulent motions generated by cylinders and the instantaneous turbine power. More specifically, it shows how the large dominant turbulent scales of incoming flow affect the spectral characteristics of turbine power, i.e, determining the level and trend of the turbine power spectrum. Comparisons reveal that there are two critical frequencies recognisable in the turbine power spectrum: the first one, close to the turbine rotational frequency, above which the coupling of upstream flow and turbine power disappears; the second one, identified for the first time and related to the dominant large-scale motions which dictate the level and trend of the turbine power spectrum. This study also shows that the strong scale-to-scale interaction between the upstream flow and turbine power reported previously does not appear at high Reynolds numbers.

1. Introduction

Wind turbines operate in a turbulent flow environment and large-scale turbulent motions cause a highly fluctuating electrical power feed into the grid. It is shown that the complex structure of turbulence dominates the spectral characteristics of power output for one single wind turbine as well as for an entire wind farm [1]. As more and more wind turbines become integrated into our electric grids, a proper understanding what causes wind turbine power output fluctuations becomes increasingly important to ensure grid efficiency and stability in future networks. Despite of its importance, the correlation of turbulent wind conditions, including extreme events and the performance of wind turbines individually or in farm is still not well understood.

There are experimental and numerical studies confirming that flow unsteadiness leads to strong temporal variations of the power output of individual wind turbines and of the entire farm. For example, Herp *et al.* [2] showed that the turbine wake expansion is highly variable, and that this variability has a negative effect on the wind-farm power optimization potential. Morales *et al.* [3] and Milan *et al.* [1] showed that power fluctuations of the turbines depend not only on the mechanical and electrical control systems but also on the wind input through analysing and modelling the effect of turbulent fluctuations on the power output of a single wind turbine and of an entire wind farm.

The above studies mainly focus on small-scale turbulent motions (high frequency) and there are few studies focusing on large-scale turbulent motions having wavelengths comparable with the turbine scale or larger (low frequency). Whilst, wind tunnel experiments [4, 5, 6] and large eddy

simulations (LES) [7] have shown that spectral densities of velocity in the wakes of turbines have a $-5/3$ slope that transit towards the -1 range at lower frequencies, wind tunnel experiments [8] and numerical studies [9] addressed an approximate $-5/3$ scaling regime for the wind farm power output possibly due to the interactions between the turbines. These studies show that there are important temporal correlations/anticorrelations between the power output of turbines in wind farms.

A good understanding of this interaction is particularly important in wind farms where the flow approaching downstream turbines will be determined by the far wake of upstream turbines which are characterised by a velocity deficit, increased turbulence intensities and a vast range of turbulence/motion scales. Andersen *et al.* [10] showed how self-organised motions or large coherent structures yield high correlations between the power productions of consecutive turbines, which can be exploited through dynamic farm control. It has been shown that complex interactions between downstream turbines affect the total-power variations of the wind farm in the intermediate to low frequency range [9]. This can significantly influence turbine farm operation with decreased power output and increased fatigue loading of devices [11]. Observations by Neustadter [12] and Barthelmie *et al.* [13] suggest that wake related losses can reduce a wind farm's average power output by 10%. It has been shown that the wind farm power output is strongly sensitive to small variations of the wind direction and it should be taken into account for the optimal control and grid integration of wind farms [14]. Numerical studies by Porté-Agel *et al.* [15], and the observations of Hansen *et al.* [16] indicate that power losses can reach over 40% for a particular single wind direction.

Increased fluctuations in power output and turbine loads can be significant in some conditions, which has also been observed in measured data [13]. Kealy [17] showed a coeffi-

cient of variations (the ratio of standard deviation to mean value) as high as 0.716 for variations in a 3-MW turbine power output in real-time caused by the variations of wind speed. Previous studies have shown that power output spectra are correlated to spectral density of the upstream flow velocity below a critical frequency close to the turbine rotational frequency but become uncorrelated at higher frequencies above that [18, 19, 20, 21]. Furthermore, Ahmadi & Yang showed that spectral density of power output correlates very well with that of velocity at the rotor plane for all frequencies at low turbulence ambient [21].

Despite many previous studies there still remains a key question on how the range of scales in the approaching turbulent flow can interact dynamically with the device and influence its ability to produce power. This is obviously of critical significance for determining the performance of a real-life wind turbine but is still not well understood despite a few studies focusing on maximising power and reducing the effect of wind on wind turbine loadings [22, 23]. Similarly, little is known about how the dynamics of large-scale coherent motions affect the rate of wake recovery of axial-flow wind turbines.

This study aims to address the above question and advance our current understanding of the flow-turbine interactions, especially due to large-scale turbulent motions at high Reynolds number. Those large-scale turbulent motions are generated in the present study by placing circular cylinders of different sizes in front of a small-scale three-bladed horizontal axis wind turbine and the main focus is on determining the effects of the large-scale motions on the turbine power fluctuations.

The paper is structured as follows: the numerical approach used in the present study and computational details are presented in Section 2. Section 3 presents temporal characteristics of predicted velocity field and power/thrust coefficients for different approaching flows and analysis of them. Concluding remarks are presented in Section 4.

2. Numerical methodology

LES is the most feasible numerical technique among all the available Computational Fluid Dynamics (CFD) methods for predicting unsteady turbulent flows accurately at the moment and in the near future [24, 25, 26] and potentially able to provide high resolution spatial and temporal information needed for this study. Actuator methods have also been demonstrated to be able to model time-dependent loading on turbine rotors [27, 28]. As addressed in [29, 30], the combination of LES and Actuator Line Modelling (ALM) has been successful in modelling turbine wakes and hence the hybrid LES/ALM approach has been employed in the present study. The CFD approach used in this study has already been validated by the authors in simulating horizontal axis wind and tidal turbines [31, 32, 21]. Figure 1 presents the predicted axial and tangential blade forces compared against experimental data for a test case already studied by the authors and presented in [21] confirming the ability and accuracy of the
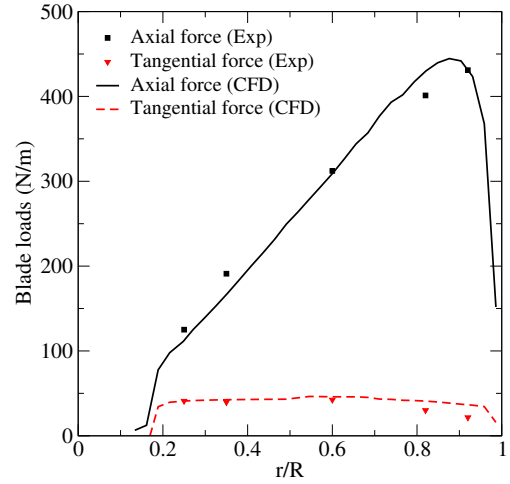

Figure 1: Axial and tangential forces of the rotor blades at wind speed of $15\,\mathrm{ms}^{-1}$ [21].

LES/ALM technique used in the present study.

2.1. Large eddy simulation

Large-scale turbulent motions (large eddies) are computed directly in LES while and small-scale motions (smaller than the mesh size) are modelled using a sub-grid-scale (SGS) model. The LES governing equations are derived by spatially filtering the three dimensional instantaneous conservation equations (Navier-Stokes). Those governing equations are fairly standard, which can be found in many textbooks and hence will be very briefly presented here.

The filtered governing equations for incompressible flow can be written in the following conservative form:

$$\frac{\partial \bar{u}_i}{\partial x_i} = 0 \tag{1}$$

$$\frac{\partial \bar{u}_i}{\partial t} + \frac{\partial (\bar{u}_i \bar{u}_j)}{\partial x_j} = -\frac{1}{\rho}\frac{\partial \bar{p}}{\partial x_i} + \nu \frac{\partial^2 \bar{u}_i}{\partial x_j^2} + \frac{\partial \tau_{ij}}{\partial x_j} + f_{i,\epsilon}$$

where the bar denotes filtered variables and $f_{i,\epsilon}$ is the body force obtained from the ALM technique described briefly below in Section. 2.2. The sub-grid scale turbulent stresses are modelled using an SGS eddy viscosity as:

$$\tau_{ij} = -\nu_t \left(\frac{\partial \bar{u}_i}{\partial x_j} + \frac{\partial \bar{u}_j}{\partial x_i} \right) + \frac{2}{3} k \delta_{ij} \tag{2}$$

where ν_t and k denote the eddy viscosity and SGS kinetic energy respectively which are obtained in the present study using a one-equation eddy viscosity model where an extra transport equation for the SGS kinetic energy [33] is solved. The CFD code employed in the present study is OpenFOAM [34].

2.2. Actuator line modelling

The turbine blade geometry is not directly resolved in the present study and its effects on the flow field are modelled using the ALM method originally developed by Sørensen & Shen [35]. Rotating actuator lines are used to represent turbine blades in the ALM technique, with body forces equal
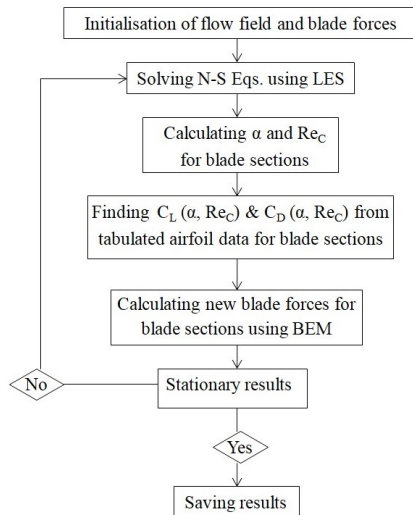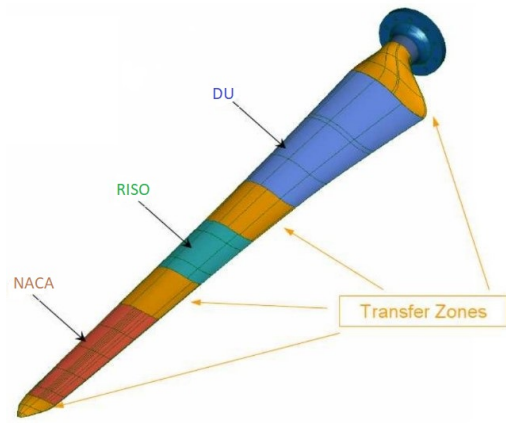
Figure 2: The hybrid LES/ALM methodology.

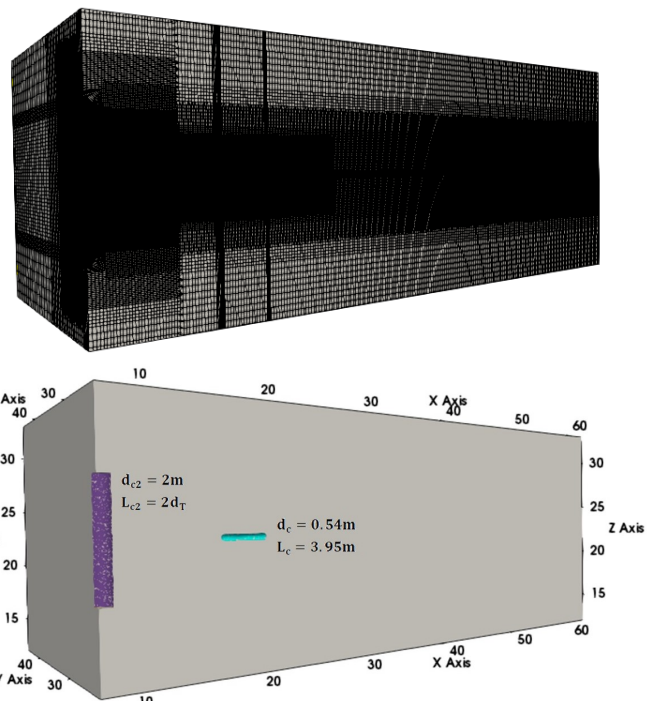Figure 3: The blade geometry [37].

Figure 4: A perspective view of the computational mesh (top) and domain configuration (bottom) at the streamwise and transverse vertical centre planes of upstream cylinder for TC2. Scales are in meter.

and opposite to the lift and drag forces experienced by the turbine blades being distributed along those rotating actuator lines. The computational procedure is as follows:

- The LES governing equations are solved over the whole computational domain initially at each time step to obtain the flow field.

- The computed flow field and the blade geometry combined with available tabulated 2D aerofoil data, i.e., C_L and C_D as functions of Reynolds number and angle of attack are used to calculate the forces at each blade section.

- 3D rotational effects are accounted for through a correction factor introduced by Shen *et al.* [36] being applied on the computed 2D forces.

- The corrected body forces are then projected smoothly along the rotating actuator lines and neighbouring mesh points using a Gaussian function to avoid singular behaviour and numerical instability.

The Gaussian cut-off parameter in the current study is set to be a constant and has a value between 2 and 3 cell sizes [29]. Figure 2 presents a flowchart summarising the hybrid LES/ALM methodology. Details of the ALM technique employed in the present study are given elsewhere [31, 32].

2.3. Computational domain

In present study, the computations of a three-bladed horizontal axis small scale wind turbine with a diameter of $d_T = 4.5$ m under three different approaching flows have been carried out using the hybrid LES/ALM technique. For the first case, the model configuration and flow conditions conform to the experimental set up of the European Union project 'MEXICO', Mexnext (Phase 1) [38, 39]. This case is referred to as the benchmark test case, denoted as TC1.

In the MEXICO turbine, each blade is composed of a cylinder, the inner 4.4 % of the span; a DU91-W2-250 aerofoil, from 11.8 % to 40 % span; a RISØ A1-21 aerofoil, from 50 % to 62 % span and a NACA64-418 aerofoil, from 72 % to 100 % span, with three transitional zones between the aerofoils. Figure 3 presents the blade geometry used in the experiments. Since the 2 D characteristic data of the RISØ aerofoil are very different from those of the other two aerofoils and as a consequence, the measured 2 D aerofoil data do not correspond to the actual characteristics of the rotor, in the middle of the blade, the aerofoil data modified and recommended by Shen *et al.* [36] are used in the present study.

The configurations of the second and third cases, denoted as TC2 and TC3, are different from that of the first case as a circular cylinder of different size is placed vertically

Table 1
Test cases with a cylinder located at the turbine upstream

	TC2				TC3		
d_{C2}	L_{C2}	Δ_2	Re_{C2}	d_{C3}	L_{C3}	Δ_3	Re_{C3}
1 m	9 m	8 m	1.04×10^6	2 m	9 m	10 m	2.09×10^6

at the upstream of the turbine to generate large-scale motions (coherent structures) in the approaching flow. Those two cases are specifically designed to study how well defined and energetic coherent structures of varying scale relative to the turbine size can affect the performance of the turbine. For the cases TC2 and TC3, in each case one cylinder is vertically placed on the vertical centre plane at the turbine upstream. Table 1 presents the cylinders' lengths and diameters, their locations and cylinder diameter-based Reynolds numbers, Re_C, for both test cases TC2 and TC3. In fact, in TC2 a cylinder with the length of $L_{C2} = 2d_T (= 9\,\text{m})$ and diameter of $d_{C2} = 1\,\text{m}$ is vertically located at the turbine upstream with a distance $\Delta_2 = 8d_{C2} (= 8\text{m})$ from it. Similarly, in TC3 a cylinder with the length and diameter of $L_{C3} = 2d_T (= 9\,\text{m})$ and $d_{C3} = 2\,\text{m}$ respectively is vertically placed at a distance $\Delta_3 = 5d_{C3} (=10\text{m})$ upstream the turbine. The cylinder diameters ($d_{C2} = 1\,\text{m}$ and $d_{C3} = 2\,\text{m}$) have been chosen to ensure that large coherent structures with length scales comparable to the turbine diameter can be generated downstream of the cylinders and the vortex shedding frequencies of cylinders are below the turbine rotational frequency. The cylinder length ($2\,d_T$) and locations upstream of the turbine ($8\,d_{C2}$ and $5\,d_{C3}$) are determined to make sure the cylinder wakes would affect the entire turbine rotor swept area. The cylinders diameters and their upstream locations have been selected based on some numerical tests together with the findings reported in [20].

As mentioned above that the turbine blades are not resolved directly but modelled using the ALM technique while the tower is ignored and the nacelle is replaced by a cylinder with the same length and diameter [37]; $L_C = 3.95\,\text{m}$ and $d_C = 0.54\,\text{m}$. Figure 4 shows a perspective view of the computational mesh and the domain cut at the streamwise and transverse vertical centre planes of upstream cylinder for TC2. The bottom picture in Figure 4 shows clearly positions of the vertical cylinder upstream of the turbine and the horizontal cylinder representing the nacelle in the computational domain.

The simulations have been performed for three different approaching flows at a free stream wind speed of $U_\infty = 15\,\text{ms}^{-1}$ and a clockwise rotational speed $\Omega = 424.5\,\text{rpm}$ when looking downstream. The corresponding tip speed ratios and turbine diameter-based Reynolds numbers are $\text{TSR} = 6.7$ and $Re_T = 4.7 \times 10^6$ respectively for all simulations. The axial, vertical and spanwise sizes of the computational domain are $14\,d_T \times 10\,d_T \times 10\,d_T$. Cartesian structured meshes of 5.25×10^6, 8.38×10^6 and 12.54×10^6 grid points with a resolution nearly $d_T/60$ in the turbine plane are used for cases TC1, TC2 and TC3 respectively. Previ-

ous relevant numerical studies [35, 36] showed that a mesh size equal to $d_T/60$ is sufficient to obtain grid independent results for the LES/ALM simulations. For all simulations, the rotor centre is located on the intersection of horizontal and vertical centre planes of the computational domain with a distance $4\,d_T$ from the inlet. The time step is chosen to be $500^{-1}\,d_T/U$ to ensure a good temporal resolution [36, 40]. Each run allows air to get through the domain six times (six flow through times) in order to reach statistically stationary flow conditions. The statistics are then averaged for the last $\frac{2}{3}$ total run time (four flow through times) to remove the effect of initial transience and obtain statistically stationary mean results. The simulations were run for 5263, 9332 and 17190 core-hours for cases TC1, TC2 and TC3 respectively. The upstream cylinder boundary layers are resolved using very high resolution meshes with $y^+ \leq 1$ for the nearest wall cells to capture vortex shedding accurately so that proper large scale coherent structures can be generated. However, resolving the boundary layer of cylinder modelling the nacelle does not really have any influence on the flow field in this study and there is no point using a very fine mesh which will increase computational cost. Therefore, a wall model developed based on the Spalding's law [41] is adopted near the solid surface of cylinder representing the nacelle, with the y^+ being approximately 12 for the nearest wall cells.

For all simulations, because of low turbulence conditions in the benchmark experiment, a divergence-free organized perturbations superimposed upon a uniform velocity profile are used at the inlet boundary and the zero normal gradient is applied for the velocity at the outlet. At the upstream boundary, the normal pressure gradient is set to be zero and a constant pressure is applied on the downstream boundary. The four side walls are treated as periodic boundaries and no slip wall boundary condition is applied on the cylinders surfaces.

3. RESULTS AND DISCUSSION

Time series of predicted velocity field and power output are presented and compared in the frequency domain for the three test cases to investigate how energetic coherent structures of varying scale relative to the turbine size affect the turbine performance. As mentioned above, the first case (TC1) with no cylinder is referred to as the benchmark test case and numerical results obtained for two other cases are analysed and evaluated with respect to it. The numerical results of the first case, TC1, have already been validated against experimental data in the author's previous work [21] and hence no more validation will be presented here.

3.1. Energetic coherent motions

Figure 5 presents iso-surfaces of the second invariant of the velocity-gradient tensor (Q) coloured by the mean velocity, showing the instantaneous flow structures for the three cases. The middle and bottom figures depict the flow structures for the cases (TC2 and TC3) with circular cylinders of diameters 1 m and 2 m placed at positions $8\,d_{C2}$ and $5\,d_{C3}$ upstream of the turbine respectively. It can be seen clearly
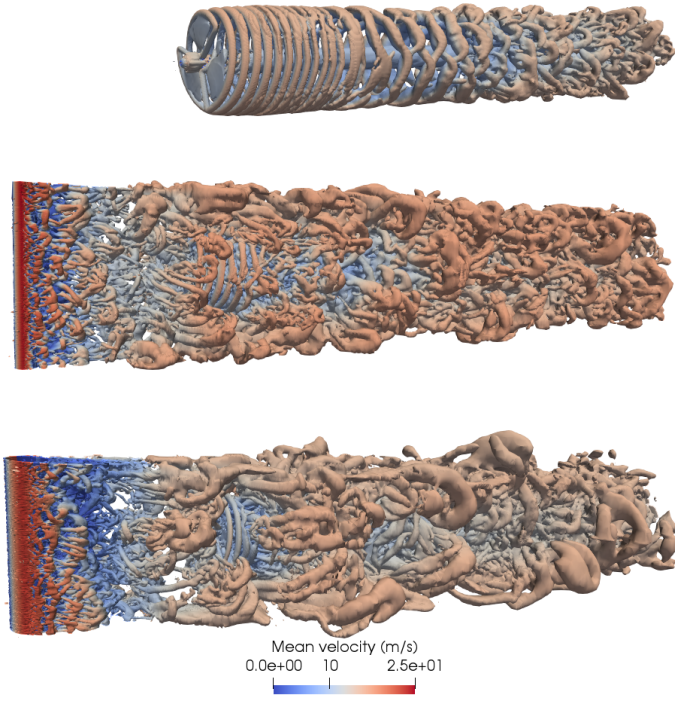
Figure 5: Instantaneous view of vortex structures in the flow field coloured by the mean velocity for three cases with no cylinder (top), small cylinder (middle) and large cylinder (bottom) in the domain.

Figure 6: Instantaneous velocity field at the horizontal centre plane of turbine for three cases with no cylinder (top), small cylinder (middle) and large cylinder (bottom) in the domain.

that large scale turbulent eddies have been generated in the approaching flow by locating circular cylinders of different sizes at the turbine upstream for TC2 and TC3 so that the interaction between the large scale motions and the instantaneous turbine power can be investigated. It is worth noting that for the case without the cylinder TC1, as mentioned in Section 2.3, the flow approaching the turbine is characterised by a low turbulence intensity whereas for TC2 and TC3 the approaching flows are highly turbulent due to the presence of energetic large-scale motions generated by the cylinders upstream.

Figure 6 presents the instantaneous velocity field at the hub height horizontal plane for the three cases and the cylinder and turbine positions are clearly shown as well. As can be seen from the middle and bottom frames of Figure 6, the wake produced by the cylinder develops into a highly turbulent flow with a broad range of scales but dominated by large-scale coherent structures due to the vortex shedding from the cylinder. Whereas for TC1 (top frame) the turbine experience an incoming flow with a low turbulence intensity confirming what is observed in Figure 5. It is worth pointing out that the characteristics of large-scale motions produced in cases TC2 and TC3 are not the same due to different cylinder diameters and are thus expected to have different impacts on the turbine performance.

In this study, to address the characteristics of large scale motions generated by the cylinders quantitatively and investigate how the range of length scales in the approaching flow
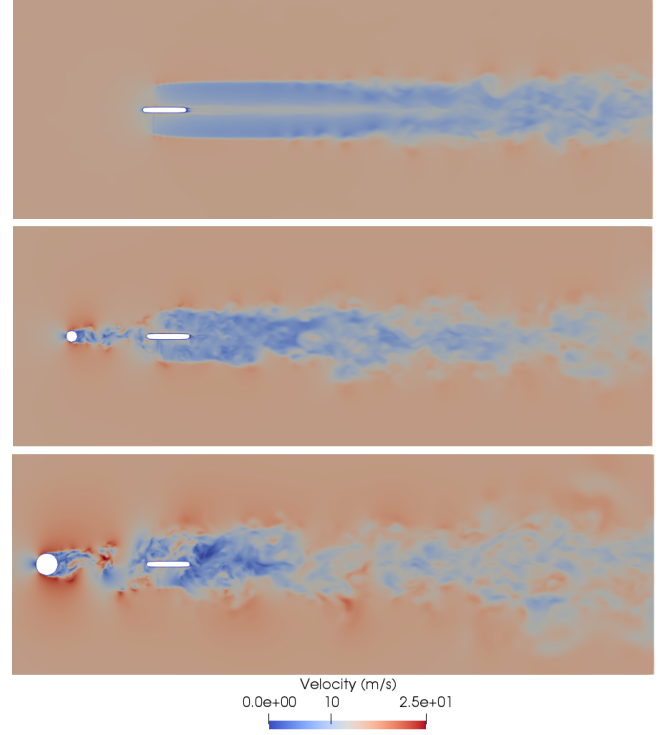
can influence the turbine power output, the power spectral densities of upstream/downstream velocity and power output presented and compared. The power spectral density (PSD) is a real, non-negative and even function defined as [42]

$$S_{xx}(f) = \lim_{t_0 \to \infty} \frac{E[|X_{t_0}(f)|^2]}{2t_0} \tag{3}$$

where $X_{t_0}(f)$ presents the the Fourier transform of the velocity or power fluctuations.

Figure 7 presents spectral densities of streamwise and transverse velocity components, v_x and v_y, for the cases TC2 and TC3 (1 d_T upstream and $d_T/8$ downstream of the turbine) at the top and bottom frames respectively, comparing with those of the case TC1. In Figures 7 to 14, upst and dnst denote upstream and downstream respectively. The frequency in the figure is normalised by the turbine rotational frequency, f_T. One major difference observable between the spectral densities (1 d_T upstream of the turbine) for TC1 and the other two cases is that the turbulent kinetic energy level is very low for TC1 because of its low turbulence intensity as shown in Figures 5 and 6.

For the case TC3, spectral densities show a peak at the frequency of 0.2 f_T for both velocity components at both upstream and downstream of the turbine while the spectral densities of the velocity components for the case with no cylinder TC1 do not show a similar peak at this frequency. This peak is due to the circular cylinder vortex shedding which leads to the generation of large-scale coherent structures ap-
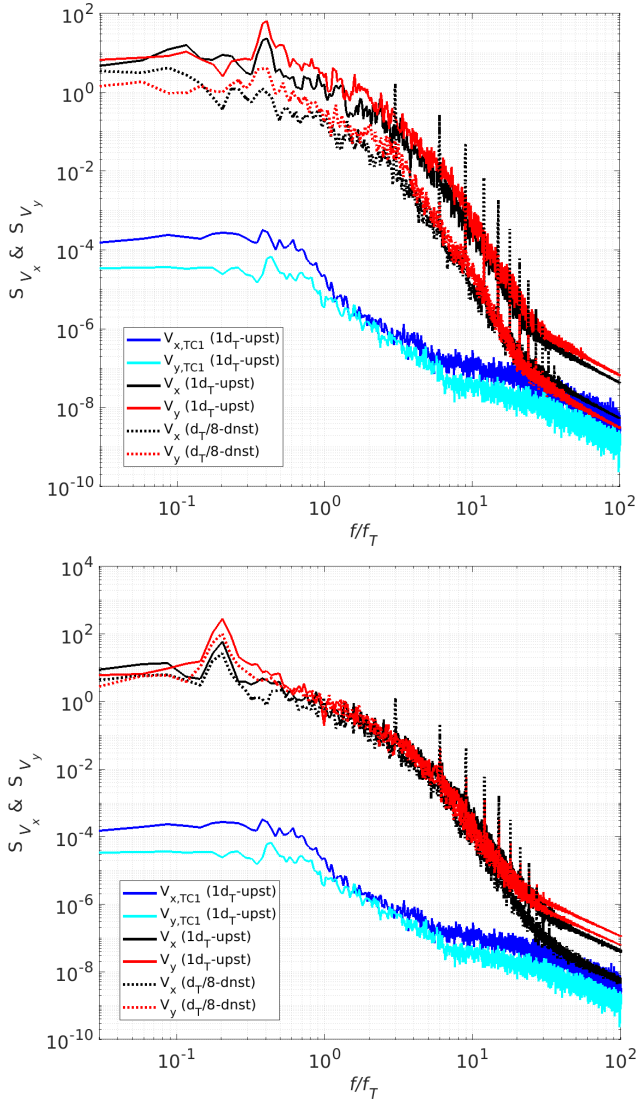
Figure 8: Spectral coherence between upstream and downstream velocity components; streamwise: black line, transverse: red line.

Figure 7: Comparing spectral densities of streamwise and transverse velocity components at the turbine upstream and downstream between cases TC1 and TC2 (top) between cases TC1 and TC3 (bottom).

proaching the turbine. The presence of the peak at $0.2 \, f_T$ (vortex shedding frequency) in the spectral densities at both upstream and downstream of the turbine with the same order of magnitude strongly indicates that large-scale coherent structures generated by the cylinder have not only reached the turbine but also passed it before breaking completely down to smaller scale structures. This situation provides a great opportunity to investigate how large-scale and energetic motions can affect the wind turbine performance at high Reynolds number flows, and especially whether "the strong scale-to-scale interaction" between the approaching flow characteristics and the instantaneous turbine power output reported by Chamorro *et al.* [20] for tidal turbines working at low Reynolds number flows also exists at high Reynolds numbers.

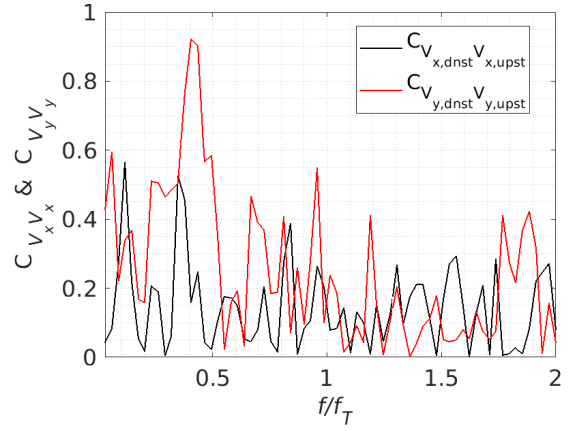A close look at the variations of spectral densities against

frequency for TC3 reveals that the spectral densities stay more or less constant at frequencies below the vortex shedding frequency and then start to decrease monotonously at frequencies higher than that. This is likely due to the large-scale coherent structures breaking down and transferring energies through this process to smaller ones. Comparing spectral densities of velocity components between cases TC1 and TC3 shows how the energetic large-scale coherent motions modify the energy contents in different scale of velocity fluctuations and its variation trend over a broad range of scales.

The top frame of Figure 7 presents spectral densities of velocity components for TC2 at both turbine upstream and downstream, and similar to TC3, a peak at frequency of $0.4 \, f_T$ is clearly visible in the spectral densities of streamwise and transverse velocity components at the turbine upstream. However, this peak disappears downstream of the turbine contrary to what happens in TC3 where the peak (at $0.2 \, f_T$) is still clearly observable downstream of the turbine. This could imply that in TC2, large-scale coherent structures produced by the cylinder break down to smaller ones sooner than in TC3. Since mesh resolutions for both cases are approximately the same and Re_{c2} is also lower than Re_{c3}, the faster breaking down of large scales structures in TC2, can not be related to the simulation inaccuracy. The most likely reason for this is due to the smaller cylinder diameter ($1 \, d_T$) in TC2 and hence the dominant large-scale coherent structures are smaller than those generated in TC3, and also the energy contents of those structures are lower than those in TC3, making them more susceptible to breaking down and hence disappearing sooner. It is notable that because of this, in TC2 the level of energy for both streamwise and transverse velocity components at the downstream are considerably less than those at the upstream contrary to what seen in TC3. On the other hand, a relative longer distance selected in TC2 ($8 \, d_{C2}$ vs. $5 \, d_{C3}$) is another possible reason why those large-scale structures disappear downstream of the turbine. This relatively longer distance is needed to cover the rotor swept area as much as possible by the developed cylinder

wake. Comparing spectral densities of velocity components between cases TC1 and TC2 confirms the key role of the energetic large-scale coherent motions in modifying the energy contents in different scale of velocity fluctuations and its variation trend over a broad range of scales.

Alternative way of comparing the flow characteristics at the upstream and downstream of the turbine can be derived from the spectral coherence between two quantities. A dimensionless parameter bounded between zero and 1, termed as spectral coherence, C_{xy}, is defined as:

$$C_{xy} = \frac{|S_{xy}(f)|^2}{S_{xx}(f)S_{yy}(f)} \qquad (4)$$

where f denotes the frequency, $S_{xx}(f)$ and $S_{yy}(f)$ present the spectral densities of quantities x and y respectively and $S_{xy}(f)$ is the cross-spectral density between x and y. Figure 8 presents the spectral coherence between streamwise velocity (black line) and transverse velocity (red line) components at locations upstream and downstream for TC2. As can be seen from the figure, although the spectral coherence between streamwise velocity at the upstream and downstream is low (about 0.2) at the frequency of $0.4\,f_T$, the spectral coherence between transverse velocity at the upstream and downstream is very high (about 0.94) at this frequency which exhibits the signature of large-scale coherent structures produced by the cylinder behind the turbine. Whilst, this indicates that dominant fluctuations experience different decay rates at different directions, it still confirms that the turbine have experienced energetic coherent motions produced by the cylinder justifying TC2 as a good case to investigate the interactions between large-scale coherent motions in the approaching flow and the instantaneous turbine performance at high Reynolds number flows.

3.2. Turbine power fluctuations

Previous studies [1, 2, 3] have shown that flow variability can affect the power output of individual wind turbines and of the entire farm. For example, as addressed in [18, 19, 43, 21], there is a frequency dependency between the turbine power and upstream turbulence. However, the above studies mainly focused on the influence of flow variability at high frequencies. There are few studies [20] that focus on the effects of large scale energetic motions at lower frequencies. To further investigate how large scale energetic motions influence the turbine power temporarily particularly at high Reynolds number flows, the spectral densities of the turbine power and thrust coefficients predicted for TC2 and TC3 are presented and compared with those of numerically obtained for TC1. The power and thrust coefficients are defined respectively as follows:

$$C_P = \frac{Q\omega}{\frac{1}{2}\rho A_r V_\infty^3} \qquad \text{and} \qquad C_T = \frac{T}{\frac{1}{2}\rho A_r V_\infty^2} \qquad (5)$$

where ρ is density, T, Q and ω denote the rotor thrust, torque and rotational speed respectively and A_r presents the rotor area. To investigate how large scale motions affect the
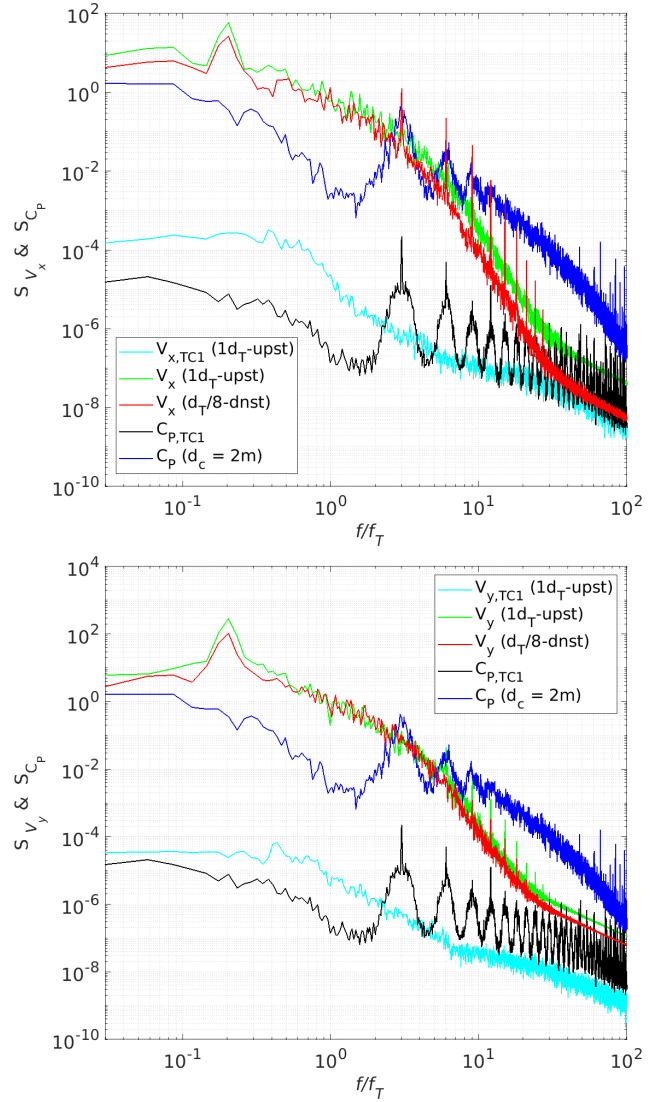

Figure 9: Spectral densities of C_P, streamwise (top) and transverse (bottom) velocity components for cases TC1 and TC3.

turbine performance, influences of the streamwise and transverse velocity components on both power and thrust coefficients are examined because of different decay rates of dominant fluctuations at different directions described before and since streamwise and tangential velocity components might have different importance in determining torque and thrust loads.

Spectral densities of predicted power coefficients for TC1 and TC3 are presented and compared in Figure 9, the spectral densities of streamwise (top frame) and transverse (bottom frame) velocity components are also plotted to facilitate comparison/analysis. It can be seen that large-scale coherent structures produced by the cylinder in TC3 not only modifies the turbulence characteristics of the flow approaching the turbine effectively as described above but also strongly affect the level of turbine power fluctuations over a broad range of scales. Comparing the variation trend of power coefficient with those of velocity components v_x and v_x at upstream for
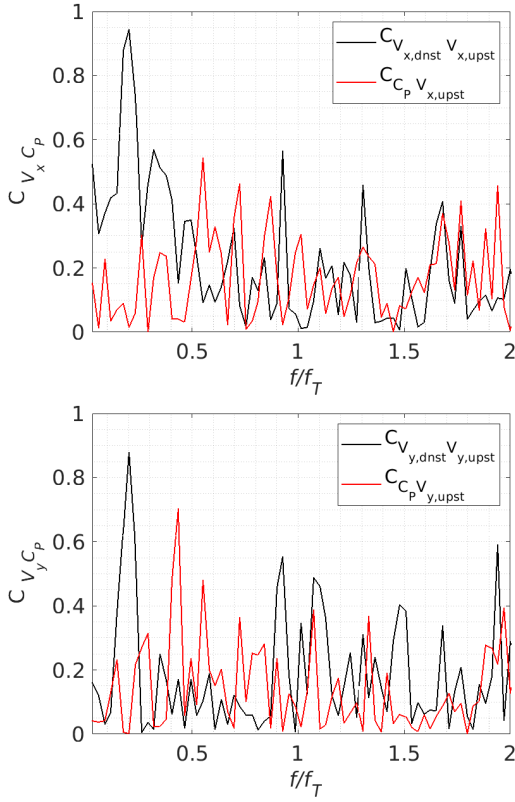
Figure 10: Spectral coherence between upstream velocity and C_P and spectral coherence between upstream and downstream velocity for the case TC3; streamwise components (top), transverse components (bottom).

Figure 11: Spectral densities of C_T, streamwise (top) and transverse (bottom) velocity components for cases TC1 and TC3.

TC3 reveals that there exists a coupling between the instantaneous turbine power and the incoming large-scale motions before a critical frequency ($\approx 1.4 f_T$) at high Reynolds number. Comparing the spectral densities of turbine power and velocity components presented for TC1 in Figure 9, show similar characteristics as those seen above for TC3, in terms of coupling and critical frequency. This kind of coupling was also reported in [19] for tidal turbines working in energetic large-scale motions at low Reynolds number. Above this frequency ($\approx 1.4 f_T$) the turbine power spectrum and the velocity spectra show quite different behaviour so that this frequency is also called the decoupling frequency in previous studies [18, 19, 21, 43]. Of course, it was already known that the turbine power spectrum reveals a signature of the blade frequency f_b ($= 3 f_T$) [44, 45].

As mentioned previously in Section 3.1 on Figure 7, the velocity spectrum trend changes at the vortex shedding frequency, i.e., the spectral density remains more or less constant at frequencies below the vortex shedding frequency and then start to decrease monotonously at frequencies higher than that. The spectral density of turbine power predicted for TC3 presented in Figure 9 shows a similar behaviour, indicating that the dominant large-scale coherent structures dictate the trend of turbine power fluctuations. This suggests a possible scale-to-scale interaction between the upstream large-scale motions and the instantaneous turbine power around
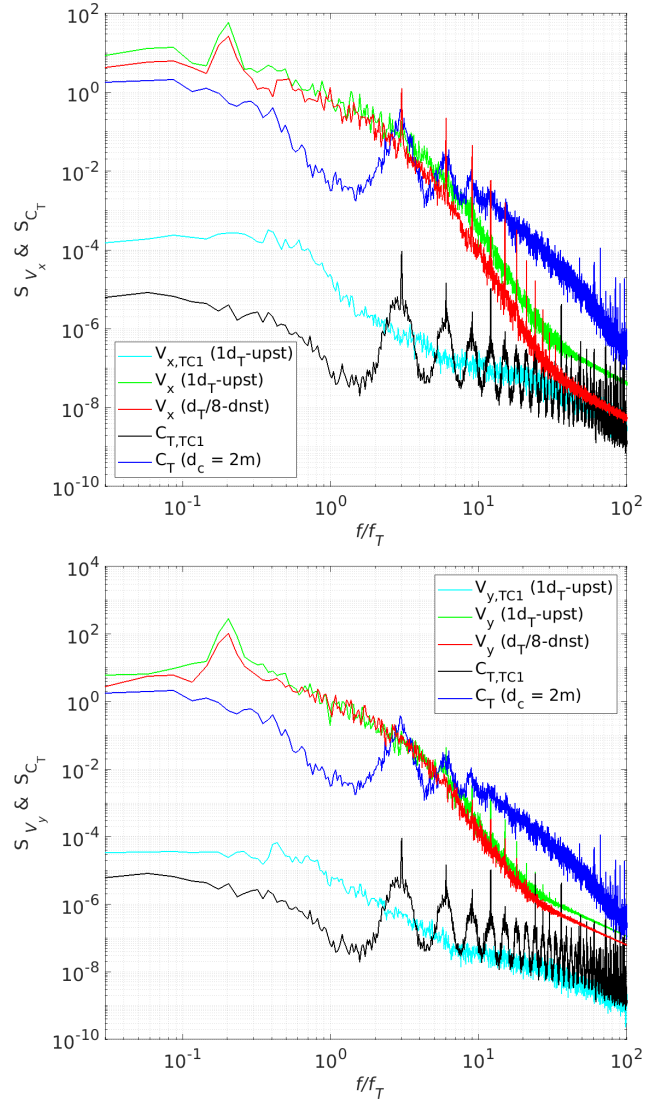
the dominant structure scales. However, contrary to that addressed in [20], the power spectrum does not show a noticeable peak around the relevant vortex shedding frequency.

To examine this point further, the spectral coherence between velocity components v_x and v_y, and the power coefficient are presented in Figure 10 and it can be seen that there are strong coherences between streamwise (top frame) and transverse (bottom frame) velocity components at locations $1\,d_T$ upstream and $d_T/8$ downstream of the turbine at the vortex shedding frequency ($0.2 f_T$). However, no considerable coherence is recognisable from the spectral coherence of the power and upstream velocity components at this frequency. In other words, the high values of coherence for velocity components confirm that large-scale motions have passed through the turbine plane but the low value of coherence between the upstream velocity and turbine power reveals no signature of the dominant motion scale in the tur-
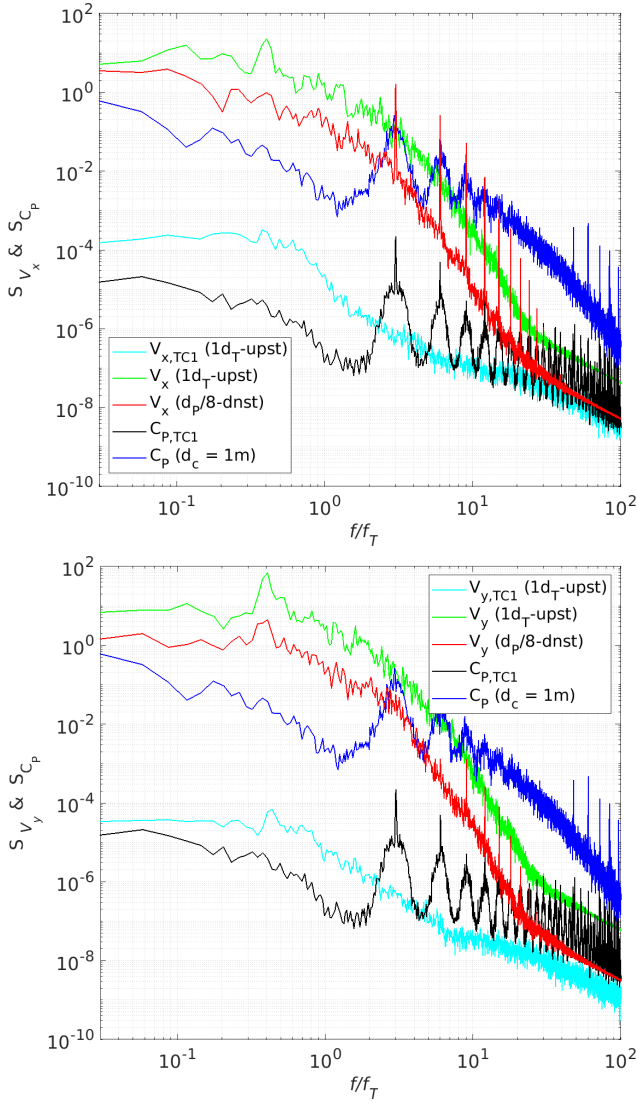
Figure 12: Spectral densities of C_P, streamwise (top) and transverse (bottom) velocity components for cases TC1 and TC2.

Figure 13: Spectral coherence between upstream velocity and C_P and spectral coherence between upstream and downstream velocity for the case TC2; streamwise components (top), transverse components (bottom).

bine power spectrum. This means that "the strong scale-to-scale interaction" between the upstream flow velocity and the turbine power addressed in [20] for tidal turbines working at low Reynolds number flows ($Re_T = 1.7 \times 10^5$) does not appear at high Reynolds number flows ($Re_T = 4.7 \times 10^6$) investigated in the present study. It is notable that, as reported by Chamorro *et al.* [20], there were nine experiments during their study and the existence of the strong scale-to-scale interaction was confirmed in one experiment only. To the author's best knowledge, there is also no other published numerical/experimental work confirming such a scale-to-scale interaction between the upstream flow velocity and the turbine power at low or high Reynolds number flows. Therefore, further studies are required to clarify this point.

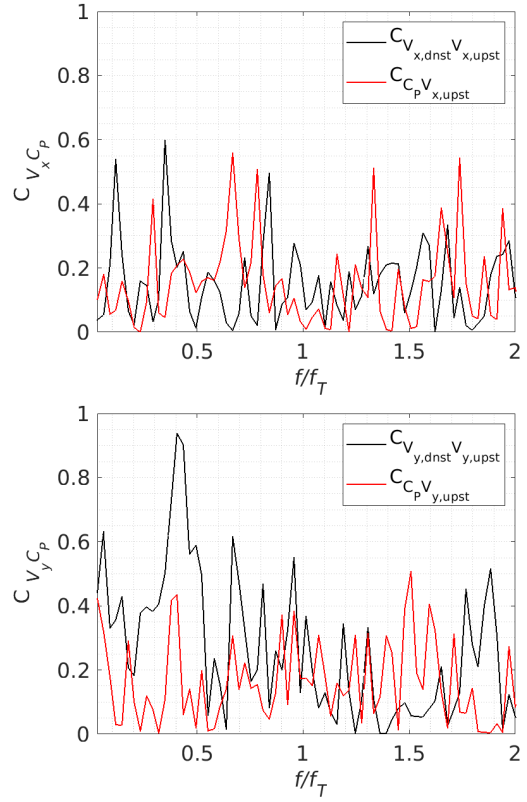Figure 11 shows the spectral densities of thrust coefficients for TC1 and TC3, and also spectral densities of stream-wise (top frame) and transverse (bottom frame) velocity components. It can be seen that the thrust spectra are similar to the power spectra shown in Figure 9 and hence more or less the same conclusion presented above with respect to Figure 9 would be drawn from the comparison shown in Figure 11 .

Spectral densities of the turbine power coefficient, C_P for TC2 with a cylinder of diameter 1 m and TC1 without a cylinder are presented in Figure 12. Spectral densities of streamwise (top frame) and transverse (bottom frame) velocity components are also depicted to provide a better view on how the incoming flow influences the turbine power characteristics. It can be seen that, similar to TC3, the turbine power fluctuations levels have strongly been affected over a broad range of scales by the large-scale motions generated from the cylinder vortex shedding. A comparison between the spectral densities of C_P and velocity components v_x and v_y at the turbine upstream location shows a strong coupling between them at low frequencies and reveals how dominant coherent structures in the approaching flow dictate the spectra trend around the vortex shedding frequencies ($\approx 0.4 f_T$) suggesting a possible scale-to-scale interaction, similar to what found for TC3 with a larger cylinder diameter. Also, a critical frequency at about $1.3 f_T$ is clearly observed for TC2 in Figure 12 similar to those seen for TC1 and TC3 in Figure 9, in which there is a coupling between the instantaneous turbine power and the upstream velocity components
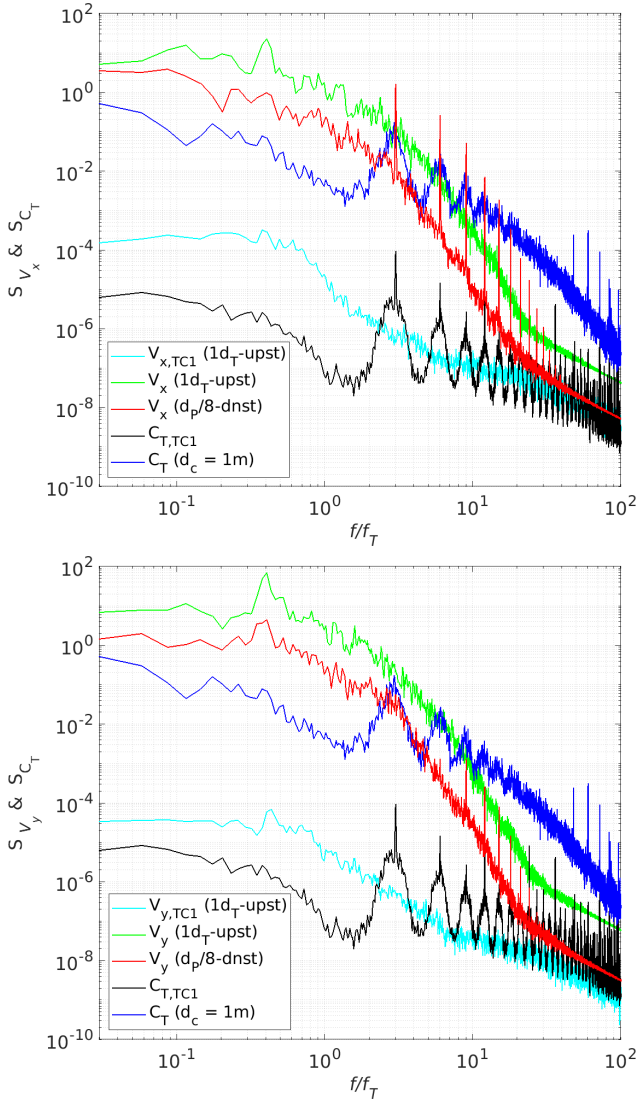
Figure 14: Spectral densities of C_T, streamwise (top) and transverse (bottom) velocity components for cases TC1 and TC2.

Figure 15: Phased-averaged C_P (top) and C_T (bottom) for cases TC1, TC2 and TC3 for one turbine revolution.

Table 2
Statistical characteristics of C_P and C_T

Cases	$C_{P,avg}$	$C_{P,max}$	$C_{P,\sigma}$	$C_{T,avg}$	$C_{T,max}$	$C_{T,\sigma}$
TC1	0.397	0.28%	0.10%	0.709	0.16%	0.05%
TC2	0.309	4.89%	1.56%	0.630	1.86%	0.58%
TC3	0.267	5.95%	2.04%	0.583	3.03%	1.21%

~~before it that disappear at higher frequencies.~~

As mentioned above, the decay rate of large scale coherent structures in the case with the smaller cylinder diameter (TC2) is higher than that of the case with the larger one (TC3). This higher decay rate may have a very different impact on different velocity component fluctuations as shown in Figure 13 that there is a strong coherency between the upstream and downstream transverse velocity components at the vortex shedding frequency $\approx 0.4 f_T$ but no considerable coherency is observed for v_x at this frequency. Despite this difference between TC2 and TC3, the C_P spectral density for TC2 shows a very similar behaviour to that for TC3 implying the high sensitivity of the turbine power in responding to large scale and broadband turbulence in the incoming flow.

Figure 14 presents the spectral densities of thrust coefficients for TC1 and TC2, plus the spectral densities of streamwise (top frame) and transverse (bottom frame) veloc-
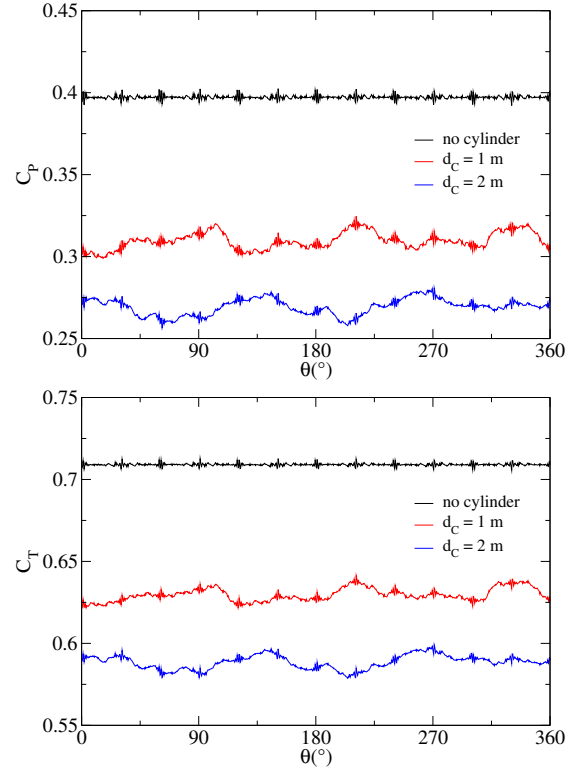
ity components. The comparison reveals a similar behaviour for the thrust to that for the power as discussed above.

The predicted mean power and thrust coefficients averaged over 81 turbine revolutions for the three cases TC1, TC2 and TC3 are shown in Figure 15. It is clearly observable that C_P and C_T are constant for TC1 without a cylinder but high unsteadiness in C_P and C_T is present for cases (TC2, TC3) with cylinders placed at the turbine upstream. This demonstrates clearly how temporal characteristics of power and thrust are strongly affected by the large-scale energetic motions approaching the turbine. The findings of this study on variations of the turbine power output caused by the energetic incoming flow concur with the empirical results of the variations in a 3-MW turbine power output in real-time presented by Kealy [17].

Table 2 presents mean, max and standard deviations values of power and thrust coefficients for the three cases. Since mean values of C_P and C_T are different for three cases, maximum and standard deviation values are presented as percentages of mean values to provide a better view of their ranges. As shown in Table 2, larger coherent structures and
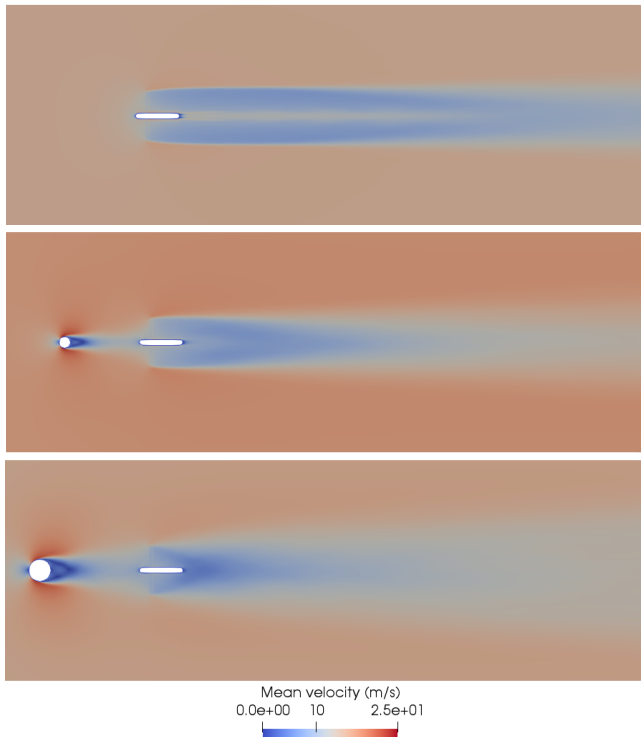
Figure 16: Mean velocity field at the horizontal centre plane of turbine for three cases with no cylinder (top), small cylinder (middle) and large cylinder (bottom) at upstream.

higher energetic motions produced by larger cylinder lead to greater amplitude and standard deviation ratios for both power and thrust coefficients. It is worth pointing out that the differences in the mean values of power output and thrust are due to different mean velocity approaching the turbine. Although the free stream velocity is the same for all cases, flow past the cylinder experiences a velocity deficit caused by the cylinder wake as shown in Figure 16 (middle and bottom frames), which is still not fully recovered at the turbine plane. As a result of this, the turbine experiences a lower mean wind speed leading to less power output and thrust. This finding suggests strongly that in wind farms downstream wind turbines should not be aligned with upstream ones and also the distance between them should be large enough so that the downstream turbines are not in the wake regions generated by the upstream turbines.

4. Conclusion

To address how the range of scales in large-scale and energetic flows approaching a wind turbine can affect dynamically the spectral characteristics of its power output, numerical simulations of a small-scale three-bladed horizontal axis wind turbine with a cylinder placed in front of it have been conducted. Large-scale energetic coherent structures of varying scale relative to the turbine size have been generated downstream of the cylinder, which modify the overall turbulence characteristics of the incoming flow and consequently affect the temporal characteristics of power output

over a broad range of scales. The cylinder diameter has been carefully selected to produce large coherent structures with length scales comparable to the turbine diameter and also to ensure that the vortex shedding frequency is in a range below the turbine rotational frequency. The cylinder length and location upstream of the turbine are appropriately determined to generate wakes affecting the entire turbine rotor swept area.

The predicted spectral densities show how modified turbulence scales because of upstream cylinder, strongly affect the spectral characteristics of turbine power in a broad range of scales. The comparison reveals that dominant large scale motions determine and dictate the level and trend of the turbine power spectrum at low frequencies suggesting a possible scale-to-scale interaction between the upstream large-scale motions and the instantaneous turbine power around the dominant structure scales. In particular, two critical frequencies have been identified in the turbine power spectrum: the first one, slightly larger than the turbine rotational frequency ($\approx 1.4 f_T$), above which the coupling of upstream flow and turbine power disappears; the second one, related to the dominant large-scale motions which determines the level and trend of the turbine power spectrum ($\approx 0.4 f_T$ for TC2 and $\approx 0.2 f_T$ for TC3). The second frequency, to the author's best knowledge, has been identified for the first time in the present study.

This study also shows that the strong scale-to-scale interaction between the upstream flow and turbine power reported by Chamorro et al. [20] at low Reynolds number does not occur at high Reynolds number flows investigated in the present work since the power spectra do not show any considerable peak around the vortex shedding frequency.

Acknowledgements

References

[1] P. Milan, M. Wächter, J. Peinke, Turbulent Character of Wind Energy, Phys. Rev. Lett. 110 (2013) 138701.

[2] J. Herp, U. V. Poulsen, M. Greiner, Wind farm power optimization including flow variability, Renew. Energy 81 (2015) 173–181.

[3] M. Morales, M. Wächter, J. Peinke, Characterization of wind turbulence by higher-order statistics, Wind Energy 15 (2012) 391–406.

[4] L. Chamorro, F. Porté-Agel, Effects of thermal stability and incoming boundary-layer flow characteristics on wind-turbine wakes: a wind-tunnel study, Boundary-Layer Meteorology 136 (2010) 273–282.

[5] W. Zhang, C. D. Markfort, F. Porté-Agel, Near-wake flow structure downwind of a wind turbine in a turbulent boundary layer, Exp. Fluids 52 (2012) 1219–1235.

[6] W. Zhang, C. D. Markfort, F. Porté-Agel, Wind-turbine wakes in a convective boundary layer: a wind-tunnel study, Boundary-Layer Meteorology 146 (2013) 161–179.

[7] M. J. Churchfield, S. Lee, J. Michalakes, P. J. Moriarty, A numeri-

cal study of the effects of atmospheric and wake turbulence on wind turbine dynamics, Journal of Turbulence 13 (2012) 1–32.

[8] J. Bossuyt, M. F. Howland, C. Meneveau, J. Meyers, Measuring power output intermittency and unsteady loading in a micro wind farm model, 34th Wind Energy Symposium, AIAA SciTech, San Diego, CA, January 2016, AIAA Pap. 2016-1992.

[9] R. J. A. M. Stevens, C. Meneveau, Temporal structure of aggregate power fluctuations in large-eddy simulations of extended wind farms, J. Renew. Sustain. Energy 6 (2014) 043102.

[10] S. J. Andersen, J. N. Sørensen, R. F. Mikkelsen, Turbulence and entrainment length scales in large wind farms, Phil. Trans. R. Soc. A 375:20160107 (2017) .

[11] S. Fransden, Turbulence and Turbulence-generated Structural Loading in Wind Turbine Clusters, PhD Thesis, Risø National Laboratory DTU, Roskilde, Denmark, Denmark (2007).

[12] H. Neustadter, D. Spera, Method for evaluating wind turbine wake effects on wind farm performance, J. Sol. Eng. 107 (1985) 240–243.

[13] R.J. Barthelmie and S.T. Frandsen and M.N. Nielsen and S.C. Pryor and P. Rethore and H.E. Jørgensen, Modelling and measurements of power losses and turbulence intensity in wind turbine wakes at middelgrunden offshore wind farm., Wind Energy 10 (6) (2007) 517–528.

[14] F. Porté-Agel, M. Bastankhah, S. Shamsoddin, Wind-Turbine and Wind-Farm Flows: A Review, Boundary-Layer Meteorology 174 (2020) 1–59.

[15] F. Porté-Agel, Y. Wu, C. Chen, A numerical study of the effects of wind direction on turbine wakes and power losses in a large wind farm, Energies 6 (10) (2013) 5297–5313.

[16] K. Hansen, R. Barthelmie, L. Jensen, A. Sommer, The impact of turbulence intensity and atmospheric stability on power deficits due to wind turbine wakes at Horns Rev wind farm, Wind Energy 15 (1) (2012) 183–196.

[17] T. Kealy, The missing parameter in renewable energy power quality analysis, i.e., the coefficient of variation: Case study of a 3-MW on-site wind turbine project in ireland, J. Clean. Prod. 280 (2021) 124699.

[18] K. B. Howard, J.S.Hu, L. P. Chamorro, M. Guala1, Characterizing the response of a wind turbine model under complex inflow conditions, Wind Energy 18 (2015) 729–743.

[19] L. Chamorro, C. Hill, S. Morton, C. Ellis, R. Arndt, F. Sotiropoulos, On the interaction between a turbulent open channel flow and an axial-flow turbine, Journal of Fluid Mechanics 716 (2013) 658–670.

[20] L. Chamorro, C. Hill, V. S. Morton, B. Gunawan, R. E. A. Arndt, F. Sotiropoulos, Effects of energetic coherent motions on the power and wake of an axial-flow turbine, Physics of Fluids 27 (2015) 055104.

[21] M. H. B. Ahmadi, Z. Yang, Numerical study of the coupling between the instantaneous blade loading/power of an axial wind turbine and upstream turbulence at high Reynolds numbers, Energy 207 (2020) 118167.

[22] Caselitz, P. and Kleinkauf, W. and Krueger, T. and Petschenka, J. and Reichard, M. and StÃűrzel, K., Reduction of fatigue loads on wind energy converters by advanced control methods, In Proceedings of European Wind Energy Conference Dublin, Ireland, 1997, pp.555–558.

[23] L. Y. Pao, K. E. Johnson, A tutorial on the dynamics and control of wind turbines and wind farms, In Proceedings of American Control Conference St. Louis, MO, USA, July 2009.

[24] A. Jimenez, A. Crespo, E. Migoya, J. Garcia, Advances in large eddy simulation of a wind turbine wake, J. Phys. Conf. Ser. 75 (1) (2007) 012041.

[25] Z. Yang, Large eddy simulation: Past, present and the future, Chinese Journal of Aeronautics 28 (2015) 11–24.

[26] M. Calaf, C. Meneveau, J. Meyers, Large eddy simulation study of fully developed wind turbine array boundary layers, Phys. Fluids 22 (1) (2010) 015110.

[27] J. N. Sørensen, C. W. Kock, A model for unsteady rotor aerodynamics, J. Wind Eng. Ind. Aerodyn 58(3) (1995) 259–275.

[28] C. Masson, A. Smaili, C. Leclerc, Aerodynamic analysis of HAWTs operating in unsteady conditions, Wind Energy 4 (1) (2001) 1–22.

[29] N. Troldborg, Actuator Line Modelling of Wind Turbine Wakes, PhD Thesis, Technical University of Denmark, Denmark (2008).

[30] R. J. A. M. Stevens, L. A. Martínez-Tossas, C. Meneveau, Comparison of wind farm large eddy simulations using actuator disk and actuator line models with wind tunnel experiments, Renew. Energy 116 (2018) 470–478.

[31] M. H. B. Ahmadi, P. Dong, Validation of the actuator line method for simulating flow through a horizontal axis tidal stream turbine by comparison with measurements, Renew. Energy 113 (2017) 420–427.

[32] M. H. B. Ahmadi, P. Dong, Numerical simulations of wake characteristics of a horizontal axis tidal stream turbine using actuator line model, Renew. Energy 113 (2017) 669–678.

[33] S. Menon, P. K. Yeung, W. W. Kim, Effect of Subgrid Models on the Computed Interscale Energy Transfer in Isotropic Turbulence, Computers & Fluids 25 (2) (1996) 165–180.

[34] OpenFOAM, Released via the OpenFOAM Foundation, See http://openfoam.org.

[35] J. N. Sørensen, W. Z. Shen, Numerical Modelling of Wind Turbine Wakes, Journal of Fluids Engineering 124 (2002) 393–399.

[36] W. Z. Shen, W. J. Zhu, J. N. Sørensen, Actuator Line/Navier-Stokes Computations for The MEXICO Rotor: Comparison With Detailed Measurements, Wind Energy 15(5) (2012) 811–825.

[37] K. Boorsma, J. G. Schepers, Description of experimental setup, MEXICO measurements, Tech. Rep. ECN-X-09-0XX, ECN (2009).

[38] J. Schepers, H. Snel, Mexico, model experiments in controlled conditions, Tech. Rep. ECNE-07-042, Energy Research Center of the Netherlands (2007).

[39] J. Schepers, K. Boorsma, T. Cho, S. Gomez-Iradi, P. Schaffarczyk, A. Jeromin, W. Z. Shen, T. Lutz, K. Meister, B. Stoevesandt, S. Schreck, D. Micallef, R. Pereira, T. Sant, H. Aagaard Madsen, N. N. Sørensen, Analysis of Mexico wind tunnel measurements, Final report of IEA Task 29, Mexnext (Phase 1), Tech. rep., ECN, ECN-E–12-004 (2012).

[40] K. Nilsson, W. Z. Shen, J. N. Sørensen, S. P. Breton, S. Ivanell, Validation of the actuator line method using near wake measurements of the MEXICO rotor, Wind Energy 37 (3) (2015) 499–514.

[41] A. Chaudhari, Large eddy simulation of wind flows over complex terrains for wind energy applications, Ph.D. Thesis, Lappeenranta University of Technology, Lappeenranta, Finland 2014.

[42] S. L. Miller, D. Childers, Probability and Random Process, Academic Press, 2nd Edition, 2004, ISBN: 978-0-12-386981-4.

[43] G. S. Payne, T. Stallard, R. Martinez, T. Bruce, Variation of loads on a three-bladed horizontal axis tidal turbine with frequency and blade position, Journal of Fluids and Structures 83 (2018) 156–170.

[44] T. Thiringer, Frequency scanning for power system property determination-applied to a wind power grid, IEEE Transactions on Power Systems 21 (2) (2006) 702–708.

[45] J. Mur-Amada, A. A. Bayod-Rújula, Characterization of Spectral Density of Wind Farm Power Output, 9th International Conference on Electrical Power Quality and Utilisation, IEEE Xplore, Barcelona, Spain, 2007, pp. 1–6.